J. Membrane Biol. 203 41–56 (2005)
DOI: 10.1007/s00232-004-0730-7

The Journal of
Membrane
Biology

A Mathematical Model of Electrolyte and Fluid Transport across Corneal Endothelium

J. Fischbarg[1], **F.P.J. Diecke**[2]
[1]Departments of Physiology and Cellular Biophysics, and Ophthalmology, Columbia University, New York, USA
[2]Deparrment of Pharmacology and Physiology, New Jersey Medical School, UMDNJ, NJ, USA

Received: 18 August 2004/Accepted: 20 December 2004

Abstract. To predict the behavior of a transporting epithelium by intuitive means can be complex and frustrating. As the number of parameters to be considered increases beyond a few, the task can be termed impossible. The alternative is to model epithelial behavior by mathematical means. For that to be feasible, it has been presumed that a large amount of experimental information is required, so as to be able to use known values for the majority of kinetic parameters. However, in the present case, we are modeling corneal endothelial behavior beginning with experimental values for only five of eleven parameters. The remaining parameter values are calculated assuming cellular steady state and using algebraic software. With that as base, as in preceding treatments but with a distribution of channels/transporters suited to the endothelium, temporal cell and tissue behavior are computed by a program written in Basic that monitors changes in chemical and electrical driving forces across cell membranes and the paracellular pathway. We find that the program reproduces quite well the behaviors experimentally observed for the translayer electrical potential difference and rate of fluid transport, (a) in the steady state, (b) after perturbations by changes in ambient conditions HCO_3^-, Na^+, and Cl^- concentrations), and (c) after challenge by inhibitors (ouabain, DIDS, Na^+- and Cl^--channel inhibitors). In addition, we have used the program to compare predictions of translayer fluid transport by two competing theories, electro-osmosis and local osmosis. Only predictions using electro-osmosis fit all the experimental data.

Key words: Local osmosis — Electro-osmosis — Paracellular — Permeability — Transport — kinetics

Introduction

Over the years, data have been contributed on corneal endothelial function. By now, a variety of membrane proteins that could contribute to translayer transport have been located and characterized. In spite of such accumulation of detail, two major questions remain unanswered: the mode in which bicarbonate ion crosses the apical membrane, and the mechanism by which fluid is transported. One way in which these problems could be confronted would be to develop a mathematical model for corneal endothelial transport to provide an organized framework in the context of which different hypothetical alternatives could be tested against experimental observations. Prior attempts to explain endothelial transport functions have resorted to schematic diagrams of transporters and their locations (Fischbarg et al., 1985; Sanchez et al., 2002; Bonanno, 2003). Such schemes, while suitable for qualitative evaluations, were not quantitative and therefore did not have extensive predictive abilities. We have therefore formulated a model that incorporates all key transporters and channels known to exist in the endothelium and presumed to be involved in fluid and electrolyte transports across the layer. We have explored the model predictions for a series of perturbations including effects of inhibitors and changes in medium composition, and find that the model reproduces experimental observations very well. Among model variants, the one postulating an apical sodium–bicarbonate cotransporter and solute–fluid coupling via electro-osmosis is the one that produces

Correspondence to: J. Fischbarg; email: jf20@columbia.edu

Abbreviations: ENaC: epithelial sodium channel; NHE: Na^+/H^+ exchanger, sodium/hydrogen exchanger; NKCC: Na^+-K^+-2Cl transporter, sodium, potassium, two chloride transporter; N2B: Na^+-2HCO_3 cotransporter, sodium, two bicarbonate cotransporter; N3B: Na^+-3HCO_3 cotransporter; sodium, three bicarbonate cotransporter.

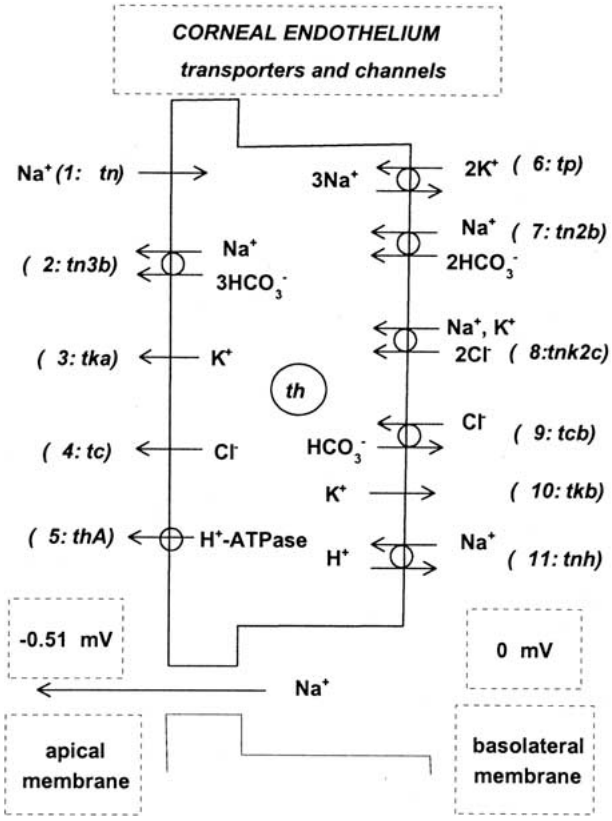

Fig. 1. Tangential section across idealized corneal endothelial cells. The illustration lists all the 11 transporters and channels that in this model contribute to either cell homeostasis or translayer transport. The ions transported are identified; the abbreviations for the turnover rates given in parenthesis are explained in Table 1.

the closest match to experimental data. The source code of the model presented is available from the authors upon request.

Model Description

The elements (channels and transporters) of the model are described in Fig. 1 and Table 1. Their distribution to either side of the corneal endothelial cell corresponds to that found immunocytochemically or deduced from experimental data. They are listed in what follows, with numbers denoting their position in Fig. 1. Their electrogenic characteristics are noted because they will be important for the model.

Apical membrane

Electrogenic: H^+-ATPase (5), sodium, three bicarbonate cotransporter (N3B) (2), potassium channel (3), chloride channel (4), epithelial sodium channel (1).

Basolateral membrane

Neutral: sodium, potassium, two chloride cotransporter (NKCC) (8), sodium/hydrogen exchanger (NHE) (11), chloride/bicarbonate exchanger (9).

Electrogenic: Sodium pump (6), sodium, two bicarbonate cotransporter (N2B) (7), potassium channel (10).

Rationale for the Polarization Scheme and the Values Chosen

There is evidence for the basolateral locations of the Na^+ pump (Kaye, Cole & Bonn, 1965), the NKCC (Jelamskii et al., 2000; Kuang et al., 2001), and the N2B (Sun et al., 2000). In addition, a Cl/HCO_3^- anion exchanger, originally assumed to be apical (Bonanno & Giasson, 1992b), has now been shown histochemically to be located in the lateral membrane domain of cells of freshly dissected corneal endothelium (Bonanno, 2003). As for K^+ channels, several have been described for corneal endothelium (Rae & Watsky, 1996; Yang et al., 2000). Some are located to the apical membrane (Rae et al., 1990); there is no reason or evidence to exclude the rest of them from the basolateral membrane. The presence of Na/H exchanger has been detected in corneal endothelium (Jentsch et al., 1988; Bonanno & Giasson, 1992a; Wigham et al., 1996), and its isoform, NHE1, has been located to the basolateral membrane (Rimmer et al., 1999). There is immunohistochemical evidence consistent with the presence of an N3B cotransporter in apical membranes of fresh and cultured endothelial cells (Diecke et al., 2004). A H^+-ATPase appears on the apical membrane based on a finding that 500 nM bafilomycin added apically inhibits fluid transport across rabbit corneal endothelium without delay (our unpublished observations).

Parameters of the Model

The model is detailed in Fig. 1, along with the symbols used for the rate of turnover of each element. The symbols begin with a *t* as a reminder that they represent each the rate of molecular turnover for the given transporters and ion channels.

The numbers for the elements correspond to those in Fig. 1. We have

(1) *tn* (sodium channel); (2) *tn3b* (sodium, three bicarbonate cotransporter); (3) *tka* (apical potassium channels); (4) *tc* (chloride channels); (5) *thA* (hydrogen–ATPase); (6) *tp* (sodium pump); (7) *tn2b* (sodium, two bicarbonate cotransporter); (8) *tnk2c* (sodium, potassium, two chloride cotransporter); (9) *tcb* (chloride-bicarbonate exchanger); (10) *tkb* (basolateral potassium channels); (11) *tnh* (sodium-hydrogen exchanger).

Using these eleven turnover rates, we assumed that the cells were in steady state and applied principles of conservation of mass; in this fashion, we constructed the system of 11 equations shown in

Table 1. System of 11 equations and 11 unknowns defining the model

	Equations	Definitions and conditions
(1)	$tp = af$	Na^+ pump
(2)	$tn2b = bf$	Na^+–$2HCO_3^-$ cotransporter
(3)	$tc = cf$	Cl^- channel
(4)	$tn = df$	Epithelial Na^+ channel
(5)	$tkb + tp + tn2b = Foc$	Basolateral K^+ channel/s
(6)	$tn2b + tp + tkb = tn + 2 \times tn3b + tc - tka$	Cellular electroneutrality
(7)	$tnk2c + 2 \times tp = tka + tkb$	K^+ conservation
(8)	$tn + tnh + tn2b + tnk2c = 3 \times tp + tn3b$	Na^+ conservation
(9)	$2 \times tn2b = 3 \times tn3b + tcb$	HCO_3^- conservation
(10)	$2 \times tnk2c + tcb = tc$	Cl^- conservation
(11)	$th = tnh + thA$	H^+ conservation

The five symbols *af*, *bf*, *cf*, *df*, and *Foc* represent flux values obtained from experimental information, as explained in the text. They were used in Eqs. 1–5. The 11 parameters that embody the model begin with a "*t*" and represent rates of turnover (or element fluxes) for the given transporters and ion channels (elements).

Table 1. With reference to that Table, for Eqs. 1–4, the turnover rates came from experimental values, so the rates were simply equated to the experimentally deduced numerical values (*af, bf, cf*, and *df*) of the corresponding element fluxes. The suffix *f* in this context implies an element flux. Of these values, *af*, *bf*, and *df* were determined from experiments in which the intracellular [Na^+] of cultured bovine corneal endothelial cells was monitored using sodium binding benzofuran isophthalate (SBFI) and inhibitors (*af*: ouabain, *bf*: DIDS, *df*: phenamil) (Kuang et al., 2004). The value of *cf* came from measurements of the reduction of fluid transport (by 14%) in the presence of the Cl^- channel inhibitor NPPB (Diecke et all al., 2004; Kuang et al., 2001). Only values of *cf* in a very narrow range provided a desired steady state, in which all the other fluxes and intracellular concentrations had reasonable values (*see below*). For Eq. 5 (Table 1), we postulated that the recirculating paracellular open-circuit current *Ioc* equaled the currents across the apical and basolateral membranes in series, that is, $Ioc = Iap = Ib1$. The value of *Ioc* was calculated from the potential difference (PD) determined across freshly mounted rabbit corneal endothelial preparations ($PD \sim 510$ μV; Fischbarg & Lim, 1974; Fischbarg, 1979) and the transendothelial total specific electrical resistance ($Rt = 20$ ohm cm^2; Fischbarg, 1979; Hodson & Miller, 1976). Since the transcellular resistance due to the two cell membranes in series is comparatively much higher than *Rt* (Lim & Fischbarg, 1981), it follows that Ioc $\sim PD/Rt = 25.5$ μA $cm^{-2} = 0.955$ μEq h^{-1} cm^{-2}. We then equated *Ioc* to the sum of the rates of the electrogenic elements in the basolateral membrane (K^+ channels plus Na^+ pump plus Na^+–HCO_3^- cotransporter. To be noted, K^+ channels and the Na^+ pump drive positive charge out of the cell, and so does the N2B cotransporter in moving 2 negative and one positive charge into the cell per cycle.

Equation 6 responds to the principle of cellular electroneutrality, for which it must be that $Ib1 = Iap$; note that for *Ib1* a positive term means positive charge going out of the cell, and for *Iap* a positive term means positive charge going into the cell. Equations 7–11 represent conservation for each given ion species (K^+, Na^+, HCO_3^-, Cl^-, and H^+). In Eq. 11, *th* represents the rate of cellular production of H^+.

The system of 11 simultaneous equations in Table 1 was solved using Mathcad® (Mathsoft, Cambridge, MA; solve block function). The solutions obtained are shown in Table 2. That Table shows also the experimental values used for parameters *af* through *df*, and the values calculated from the algebraic solutions for the unknown parameters. As can be seen there, interestingly, at the steady-state conditions assumed, the turnover of the Na^+-H^+ exchanger *tnh* is zero (there are some data that suggest that its steady-state activity is relatively low (Bonanno & Giasson, 1992a). Moreover, from Table 2, *thA* (the turnover of the apical H^+-ATPase) equals *th* (the rate of intracellular H^+ generation), and from Table 1 it can be seen that these turnover rates are present only in Eq. 11. The precise value of them is not known at present; however, as they do not influence the rest of the parameters and hence the behavior of the model, for convenience they were set at zero.

Using the turnover values of Table 2, one can calculate steady-state ionic fluxes across each one of the 11 transporters/channels in the model (Fig. 1). Transporters/channels are also called "elements" in our context. Figure 2 shows these results; bars representing fluxes are oriented according to their direction. As can be seen, the cell is transporting a substantial amount of HCO3$^-$ from basolateral to apical (stroma to aqueous), and much smaller amounts of K^+ and Cl^- in the same direction. The Na^+ flux is also substantial, but in contrast, goes in the opposite direction.

Table 2. Algebraic solutions and numerical values for all turnover rates

	Algebraic solutions for turnover rate	Values (μmol h^{-1} cm^{-2})	
		Estimated from experiments	Calculated
(1)	$tn = df$	0.532	
(2)	$tn3b = -cf + 6 \times af - 2\,df$		0.294
(3)	$tka = -Foc - 3 \times df - cf + 12 \times af$		0.327
(4)	$tc = cf$	0.162	
(5)	$thA = th$		0 (set)
(6)	$tp = af$	0.253	
(7)	$tn2b = bf$	0.456	
(8)	$tnk2c = -bf - cf + 9 \times af - 3 \times df$		0.066
(9)	$tcb = 2 \times bf + 3 \times cf - 18 \times af + 6 \times df$		0.03
(10)	$tkb = Foc - af - bf$		0.246
(11)	$tnh = 0$		

Foc = 0.955 μmol h^{-1} cm^{-2}
Equation numbers correspond to the numbers identifying the elements in Fig. 1

Figure 2 may suggest a hypothetical argument: could the cell operate instead by transporting less bicarbonate and more chloride than shown there? We found the answer negative. To expand on what was mentioned above, flux values cannot deviate very much from the values found for them without compromising the behavior of the model. To illustrate this point, Fig. 3 shows an example of the dependence of the unknown or computed parameters on the values of the known parameters. In this case the independent variable is the apical Cl^- channel turnover, which would have to be larger to make possible larger hypothetical chloride transcellular fluxes. As can be seen in Fig. 3, a small decrease of the Cl^- channel turnover from its set value shown (0.162 in our standard units) is sufficient to reverse the direction of the anion exchanger, which under normal conditions is thought to bring Cl^- into the cell. Such a reversal in turn is only possible if the $[Cl^-]_i$ would rise to unphysiological concentrations. On the other hand, assuming a larger turnover rate of the apical Cl^- channel leads to an increase in intracellular Cl^- and in turn to a reversal of the flux through the Na^+-K^+–$2Cl^-$ cotransporter to meet the steady-state conditions set by the conservation equations for the major ions and electroneutrality (Table 1). Again, this is an unphysiological condition.

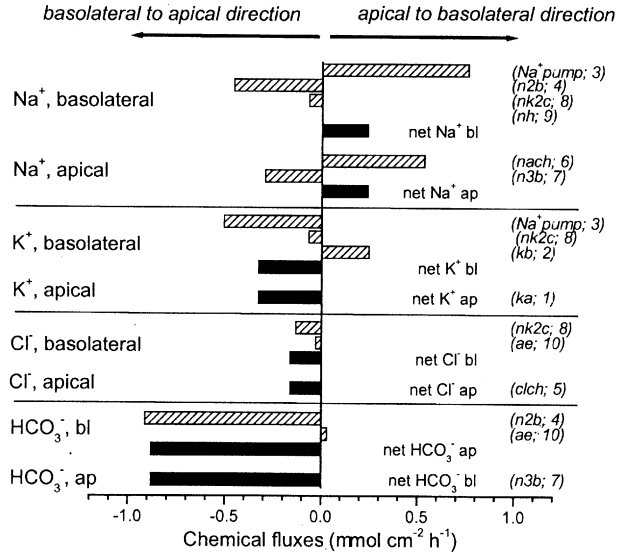

Fig. 2. Unidirectional (*hatched bars*) and net electrolyte fluxes (*black bars*) across each of the transporters/channels described in the model of Fig. 1. The values shown were obtained by solving the system of 11 linear equations listed in Table 1. For three of the fluxes (apical K^+, Cl^-, and HCO_3^-), the unidirectional fluxes are not shown, as they were equal to the net flux. Several of the 11 elements appear more than once in this figure (Na^+ pump, NaH-CO_3 cotransporters, NKCC, anion exchanger) because they carry simultaneously more than one ion species.

Kinetic Equations for the Channels and Transporters

The treatment was built upon the basis of the calculated steady-state turnover rates given in Table 2. These baseline rates were modified using kinetic terms and electrochemical gradients to adjust them to the varying surroundings, as needed.

The modifiers were of three types; the detailed expressions utilized are given in the Appendix for each case. In the first group, we developed kinetic equations based on first principles for all the cotransporters and exchangers present. For the binding steps, we employed saturation formalisms which, while relatively standard, may not have appeared before in this context in the form detailed here. For the electrogenic transporters, in addition, the equations included the effect of the transmembrane electrical potential difference on the translocation step. The results obtained were validated by separate calculations using simply electrochemical potential differences.

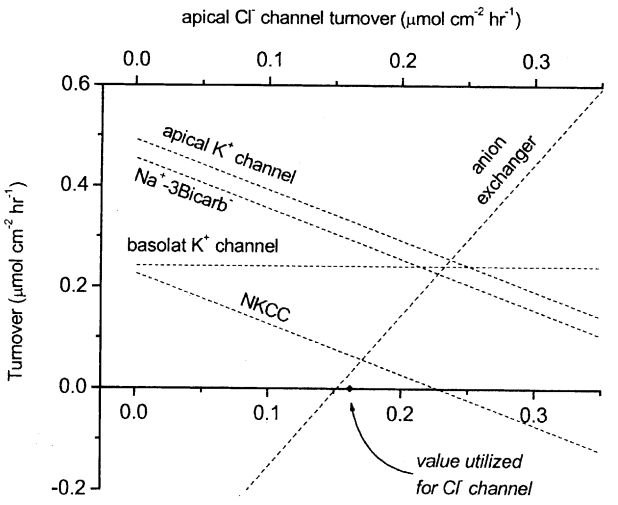

Fig. 3. The rates of turnover initially chosen for the model are all interlinked by 11 equations corresponding to conservation of mass. That system of equations was solved in the Mathcad environment. Changing the value set for the turnover for the Cl^- channel resulted in changes in the turnovers of several other elements, as the figure details.

Permeabilities for Membrane Channels and the Paracellular Pathway

A second group of equations was applied to membrane channels and to the paracellular pathway. For them, as in prior treatments (Verkman & Alpern, 1987; Hartmann & Verkman, 1990; Sohma et al., 2000), the driving forces were computed using the Goldman-Hodgkin-Katz formulation, and the permeability was computed as the ratio of the baseline turnover over the driving force. In the case of the paracellular pathway, we used free solution partial conductances weighted by the junctional relative selectivities (Lim, Liebovitch & Fischbarg, 1983). Paracellular permeabilities were calculated using the data of Lim et al., 1983; the potential differences were corrected for the liquid junction potential that solution asymmetries would have created across the endothelial layer. They were scaled to a transendothelial specific resistance value of 20 Ω cm^2. The values obtained were: P_{Na} = 6.45698E−05 cm/s; P_K = 7.74837E-05 cm/s; P_{Cl} = 3.22849E-05 cm/s; and P_{HCO3} = 3.22849E-05 cm/s. In the third group, the equations were empirical, as derived before to reproduce the kinetics of the Na^+ pump (Latta, Clausen & Moore, 1984) and the H^+–ATPase (Hartmann & Verkman, 1990).

Kinetic Constants

The apparent dissociation constants of the cell plasma membrane transporters included in the model were taken mostly from the literature, and some from our own data. Values for the NKCC cotransporter came from our experiments using cultured bovine corneal endothelial cells (Diecke et al., 2005). Table 3 summarizes the values and the sources for them.

Program Structure and Principles Used for it

There have been several precedents for the task of building an epithelial computer model (Lew, Ferreira & Moura, 1979; Latta et al., 1984; Verkman & Alpern, 1987; Hartmann & Verkman, 1990; Novotny & Jakobsson, 1996; Sohma et al., 2000;). The current treatment starts from ideas and software routines written in Basic for a preceding paper (Hartmann & Verkman, 1990), and expands it to cover a full array of transporters plus translayer fluid and electrolyte transports.

Flowchart

The sequence of programming steps is summarized in the accompanying flowchart of Fig. 4. The program begins its run at (*1*) by importing initial data from a file; this file contains initial values for the extracellular and intracellular concentrations, absolute and relative turnover values, and dissociation constants for the different transporters. Some of the initial values it utilizes are detailed in Table 4.

Primary Fluxes. The basis of the treatment are what we will call "primary transporter/channel fluxes", or "element fluxes", numbering 11. They correspond to parameters that have been called turnover rates in several preceding treatments (Hartmann & Verkman, 1990; Sohma et al., 2000). They are the ionic fluxes through given elements divided by the applicable stoichiometric coefficients of the transporters (3 for the Na^+ pump, etc.). They are related to the molecular turnovers of those transporters/channels ("elements"), since they are equivalent to molecular turnover number times density of transporters/channels divided by N_{AV}, in units of cycles × moles/(time × area). As all fluxes in this context, they have dimensions of fluxes per unit area (à la Kedem-Katchalsky; Kedem & Katchalsky, 1958), in our case "standard units" of μmol cm^{-2} h^{-1}. To be noted, the reference area is the en face or tangential area of the cells. These 11 turnover rates (or element fluxes) figure prominently in the system of 11 equations and 11 unknowns portrayed in Table 1; their calculated values (given in Table 2) are incorporated to the program code.

Driving Forces. As can be recognized, the primary turnover rates above result from driving forces applied to the different elements. Given the myriad factors involved in the driving forces, we opted for normalizing

Table 3. Dissociation constants for the transporters in the model

Transporter	$K_{0.5}$	Source
Na^+-K^+-ATPase	K_{Na} = 11.8 mM K_K = 1.4 mM	Westenfelder, Earnest & Al-Bazzaz, 1980
Na^+–3HCO_3^- cotransporter	K_{Na} = 15 mM K_{HCO_3} = 20 mM	Gross &Hopfer, 1998
Na^+–2HCO_3^- cotransporter	K_{Na} = 7 mM* K_{HCO_3} = 10.8 mM**	Peral, Calonge& Ilundain, 1995* Grichtchenko, Romero & Boron, 2000**
Cl^-/HCO_3^-exchanger	K_{cl} = 10 mM* K_{HCO_3} = 10 mM**	Kohn, Mitchell & Steinmetz, 1990* Wieth, 1979**
Na^+-K^+–2Cl^- cotransporter	K_{Na} = 21.1 mM K_K = 1.33 mM K_{cl} = 26 mM	Diecke et al., 2005
Na^+/H^+ exchanger	K_{Na} = 7.1 mM K_H = 3.8E-05 mM	Aronson, Suhm & Nee, 1983

As explained in the text, the transporters in the cell membranes are characterized by their dissociation constants (*K*m values) and the paracellular pathway has different permeabilities for the ions considered. This table shows the initial values utilized here for those parameters as the program is loaded. The program allows them to be changed if indicated. Asterisks match constants with their respective references.

all forces by dividing them by suitable reference forces, so that all driving forces become dimensionless "*drf*" parameters.

Absolute and Relative Permeabilities (Permeability Coefficients). Given the two elements above, an absolute permeability is obtained by dividing the primary flux by the corresponding normalized driving force ("*drf*"). Since the driving forces are dimensionless, the absolute permeabilities in our case will have the same dimensions as the primary fluxes, that is, standard units. These absolute permeabilities are calculated early on in the program (step (*4*) in the flowchart), using the driving forces existing at zero time. They retain their value throughout a given simulation; fluxes are updated only as the driving forces change. By contrast, the relative permeabilities are dimensionless factors, which allow one to simulate inhibition or stimulation of a given element. Our permeability coefficients correspond therefore to those in the nomenclature of Hartmann and Verkman (Hartmann & Verkman, 1990), except that ours have dimensions of fluxes for the reasons noted.

Actual Run. In flowchart step (*5*), fluxes are calculated for each electrolyte across the two cell membranes and the paracellular space. In step (*6*), conditions for the run are set: the program allows the operator to set changes in the concentrations and/or element activities typically induced by modulators (via changes in relative permeabilities), and to set the times for those changes.

Main Iteration Loop. As the flowchart shows, the program first calculates the driving forces (*drfs*). It then uses the *drfs* to update the values of transmembrane fluxes through the different elements, and the values of the transcellular and paracellular currents. After that, it computes the potential differences (*PD*s) across both sides of the cell which are required to

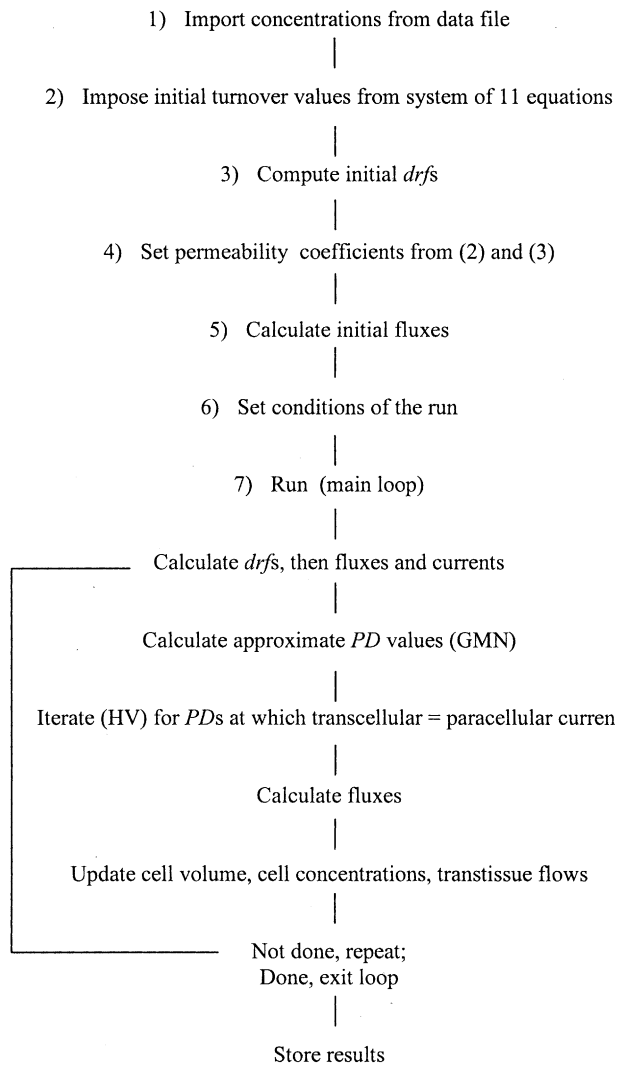

Fig. 4. Flowchart of the Basic program that implements the model. Abbreviations mean: *GMN*, Goldman-Hodgkin-Katz equation; *HV*, Hartmann-Verkman.

Table 4. Standard electrolyte concentrations and potential differences

	Intracellular concentration mmol/L	Extracellular concentration mmol/L	Potential difference mV
[Na+]	13	140.1	
[K+]	132	4.9	
[Cl−]	40	108	
[HCO3−]	37	37	
[Impenneant anion]	68	0	
V_{map}			−45
V_{mbas}			−45.51
PD (V_{mbas}-V_{map})			−0.510

V_{map}, V_{mbas}: potential differences across the apical and basolateral membranes, respectively. PD, translayer electrical potential difference. For translayer potentials, the basolateral solution is the reference. For intracellular potentials, the extracellular solution is the reference.

maintain the fluxes just computed. The algorithm to calculate the *PD*s is the heart of the program. Aside from minor adjustments, it was taken directly from the algorithm of Hartmann and Verkman (1990). It is based on electroneutrality, and it consists of a series of iterations using the nonlinear Newton's method, in which the program searches for *PD* values that minimize the differences (deltas) between the electrical currents at both membranes, and between transcellular and paracellular currents. As a condition of convergence for this subroutine, we required current deltas of less than 10^{-5} (in $\mu A\ cm^{-2}$). Given this high imposed accuracy, we modified the original algorithm so as to cut the number of required iterations by furnishing to the subroutine approximate *PD* values to start from. The "approximations" were actually very good, as they were based on the Goldman equation with the modification for an electrogenic Na^+ pump, as introduced by Mullins and Noda (Mullins & Noda, 1963; Lakshminarayanaiah, 1984, pg. 145). After the *PD*s were obtained, all fluxes into and out of the cell were calculated, and on that basis, cell concentrations and volume were updated, and the translayer chemical fluxes were computed.

Calculations of fluid transport and corneal thickness. The model computed transendothelial fluid transport for two sets of assumptions, (a) local osmosis, and (b) electro-osmosis. In (a), it was assumed that the fluid transported was isotonic with the translayer net salt flux. In (b), the fluid movement was calculated from the paracellular current and a current-fluid coupling coefficient through the paracellular path determined experimentally (2.37 $\mu m\ cm^{-2}\ \mu A^{-1}\ hr^{-1}$ (Sanchez et al., 2002). Corneal thickness changes were calculated using the calculated translayer fluid flow. In this last case, we made the following assumptions:

a) The rate of change of corneal thickness is a function of fluid movements into or out of the stroma due to the imbibition pressure driving fluid into the stroma, and to the activity of the endothelial fluid pump driving fluid out of the stroma.

b) The imbibition pressure in the stroma is zero at "maximal" hydration, corresponding to a corneal thickness of 575 μm (maximal thickness).

c) At normal corneal thickness of 350 μm (reference thickness) fluid uptake due to imbibition pressure and fluid extrusion due to endothelial transport are equal and opposite.

d) Ouabain administration causes a complete inhibition of the endothelial fluid extrusion and the resulting rate of change of stromal thickness is a measure of the fluid uptake by the stroma at that thickness and hydration pressure.

e) The imbibition pressure is thickness-dependent. The equation utilized was:

corneal thickness $(t+1)$ = corneal thickness (t) − fluid transport × sampling interval + [baseline fluid transport $(t = 0)$ × sampling interval] × {[max. thickness − corneal thickness (t)] / swelling interval}, where maximal thickness = baseline thickness + swelling interval. The usual value for the swelling interval was 225 μm.

As currently written, the algorithm follows 37 different parameters as a function of time. Included are the cellular ionic concentrations, pH, volume, membrane and translayer potential differences, the ion flows through each of the model elements, fluid transport computed assuming local osmosis and electro-osmosis, corneal thickness.

Results

Application of the Model. Steady State, Inhibitors, and Ionic Replacements

We have utilized the model to simulate transport of fluid and electrolytes under baseline conditions and under several test conditions reproducing common experimental manipulations, such as inhibition of ion transporters and channels and changes in the extracellular electrolyte environment. Where feasible, the predictions of the model have then been compared

with experimental data from the literature for in vitro rabbit corneal endothelial preparations.

Fluid and Electrolyte Transport

Under the conditions assumed here for corneal endothelial cells (Table 4) the model, as shown in Fig. 5, predicts transcellular fluxes (in μmol cm^{-2} h^{-1}) from the basolateral to the apical side (outwards) for three electrolytes: a) HCO_3^-, 0.882; b) Cl^-, 0.162; and c) K^+, 0.331. The cause of these vectorial electrolyte movements is that there are transporting elements in the basolateral membrane, bringing them into the cell (Na^+–2 HCO_3^- cotransporter, Na^+-K^+–2Cl^- cotransporter, anion exchanger and Na^+-K^+-ATPase), and also elements (Na^+–3HCO_3^- cotransporter, K^+ channels, Cl^- channels) in the apical membrane, transporting them out of the cell. The model also predicts a transcellular flux of Na^+ (0.238 μmol cm^{-2} h^{-1}) in the opposite direction, namely from apical to basolateral (inward). This flux results from apical Na^+ entry through epithelial Na^+ channels (ENaC) and subsequent extrusion across the basolateral membrane via the Na^+ pump.

The transendothelial potential difference of –0.51 mV generates a paracellular current of 25.5 μA cm^{-2} equivalent to an ion flux of 0.95 μEq cm^{-2} h^{-1}. Based on the junctional permeabilities (Lim et al., 1983) for the major ions (Na^+, K^+, Cl^-, HCO_3^-), the model computes the following partial fluxes (in μmol cm^{-2} h^{-1}) through the tight junction from basolateral to apical side: Na^+ = 0.625; K^+ = 0.022; and from apical to basolateral: Cl^- = 0.221; HCO_3^- = 0.081.

The total translayer electrolyte movements are the algebraic sums of the transcellular and the paracellular fluxes. As shown in Fig. 5, net translayer fluxes (in μmol cm^{-2} h^{-1}) are: Na^+ = 0.387; K^+ = 0.353; Cl^- = –0.059; and HCO_3^- = 0.801, where positive values indicate flux from the basolateral to the apical side. The fluid transport computed by the model for electro-osmotic coupling is 6.0 μL cm^{-2} h^{-1} and 4.9 μL cm^{-2} h^{-1} for local osmosis. Both values are within the range of values found experimentally for freshly dissected de-epithelialized cornea preparations using the Maurice-Dikstein method (Dikstein & Maurice, 1972).

Inhibitors

Ouabain. Figure 6 shows the changes in major intracellular electrolytes (Na^+, K^+, Cl^-, HCO_3^-), cell volume and fluid transport upon inhibition of the Na^+-K^+-ATPase with ouabain. After simulated ouabain application, fluid transport is immediately decreased by a small fraction. This reduction is due to the inhibition of the Na^+ pump, which contributes to

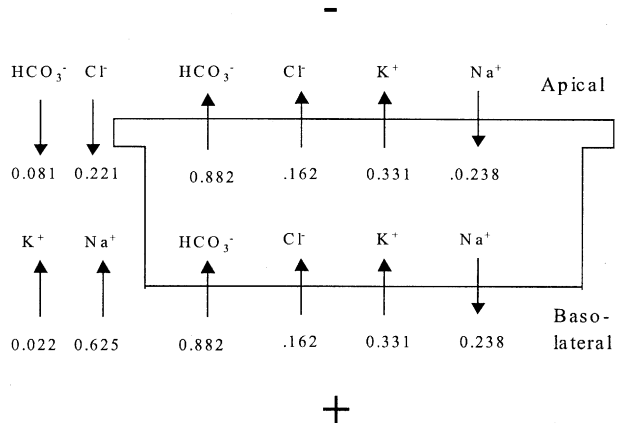

Fig. 5. Values in the drawing are computed by the program for net transmembrane and paracellular ionic fluxes in the steady-state. Values for net translayer fluxes were: HCO_3^- = 0.801 μmol cm^{-2} h^{-1} Cl^- = –0.059 μmol cm^{-2} h^{-1} K^+ = 0.353 μmol $cm^{-2}h^{-1}$ Na^+ = 0.387 μmol $cm^{-2}h^{-1}$ Positive in this case denotes from basolateral to apical.

the basolateral membrane potential and to the translayer potential difference. Following that, there is a rapid exponential increase of the intracellular [Na^+] and a decrease of intracellular [K^+]. Subsequent changes in intracellular anion concentration, an increase in [Cl^-] and decrease in [HCO_3^-], follow with a delay. The assumed existence of an impermeant intracellular anion means that the final electrolyte distribution converges to a Donnan distribution.

As a consequence of the rapid reduction of the sodium gradient and the reduction in transendothelial potential difference, the transcellular flux through the cotransporters and the paracellular fluxes go towards zero. The transendothelial fluid transport, computed either as electro-osmotic flow or as local osmosis, ceases. The model predicts a rate of corneal swelling of 50 μm h^{-1} for electro-osmotic coupling and 43 μm h^{-1} for local osmosis (*data not shown*), which is in good agreement with experimental observations on freshly dissected de-epithelialized rabbit corneal preparations using the Dikstein-Maurice method.

DIDS. DIDS (4,4′-Diisothiocyano-2,2′-stilbenedisulf- onic acid) is an inhibitor of Na^+-HCO_3^- cotransporters, anion exchanger, and of Cl^- channels and as a consequence blocks all transcellular anion flux. As can be seen in Fig. 7 (*upper panel*), there is a striking difference between the predictions of the electro-osmotic and local osmotic models. The local osmotic model predicts a reversal of the direction of fluid transport, while the electro-osmotic model predicts instead only a 50% inhibition. As can be seen, the experimental results (Kuang et al., 2004) agree with electro-osmosis, and disagree with local osmosis.

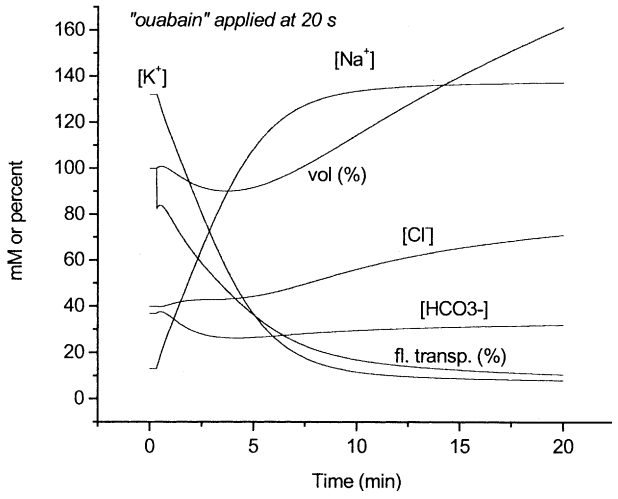

Fig. 6. Effect of ouabain on the intracellular concentrations of major electrodes (Na^+, K^+, Cl^-, HCO_3^-), cell volume, and normalized translayer fluid transport. The predictions of local osmosis and electro-osmosis for fluid transport are superimposable.

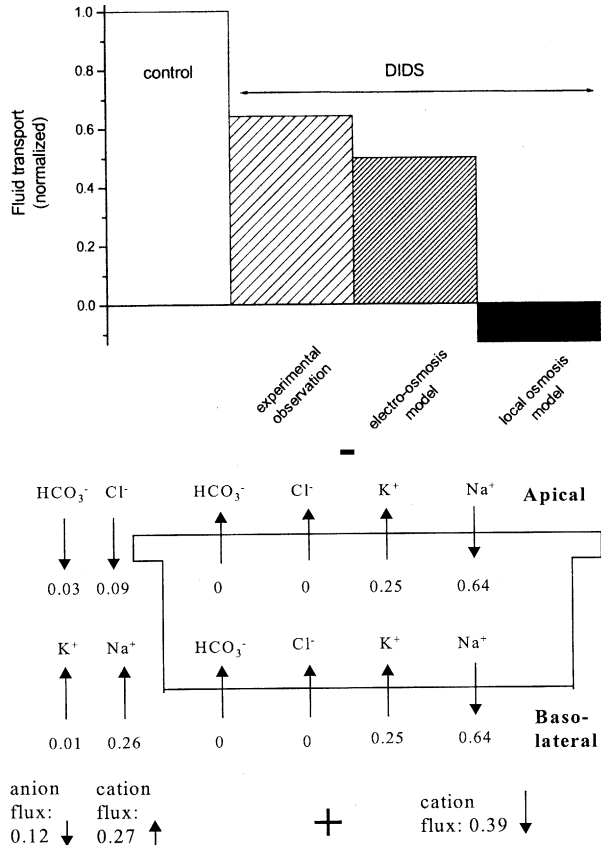

Fig. 7. Effect of DIDS on translayer fluid transport. *Top panel*: the graph compares the prediction of the two versions of the model (fluid transport by electro-osmosis or local osmosis) with an experimental observation of fluid transport as calculated from corneal thickness changes using the Dikstein-Maurice (Dikstein & Maurice, 1972) technique after 100 μM DIDS challenge (Kuang et al., 2004). *Bottom panel*: transcellular and paracellular ionic fluxes predicted by the model, assuming 99% inhibition of bicarbonate transporters and chloride channels. Numbers denote μmol cm^{-2} h^{-1}.

The explanation for this phenomenon is the following. Upon simulated DIDS addition, since the Na^+ pump remains unaffected, the model computes a remaining transendothelial potential difference of −0.21 mV or 42% of the control value (*data not shown*). This transendothelial potential difference in turn generates a paracellular cation flux from basolateral to apical. This cation flux, by electro-osmotic coupling at the junctions, would generate fluid movement, as experimentally observed (Fig. 7, *upper panel*).

In contrast, fluid transported by local osmosis would depend on net salt flow. In the presence of DIDS, the cell still transports cations from apical to basolateral (inward), but does not transport anions. By electroneutrality, this net transcellular cation flux is partially balanced by the transjunctional cation flux described above, and the remainder is accompanied a paracellular anion flux from apical to basolateral (Fig. 7, *lower panel*). Hence, there is net electrolyte flux from the apical to the basolateral side. Still, as can be seen, this net electrolyte flux does not generate fluid flow, as it would if local osmosis would take place and there would be no electro-osmosis.

Phenamil. Phenamil (3,5-diamino-6-chloro-n-[amino (phenylamino)methyl]-pyrazine carboxamide) is a specific inhibitor of epithelial Na^+ channels, and we have therefore simulated its effects by reducing the relative permeability of the Na^+ channel (*tn*). Figure 8 shows the predictions of the model, assuming fluid transport by (a) local osmosis and (b) by electro-osmosis. Phenamil inhibition does not affect net salt flux across the endothelium (*data not shown*); as a consequence, fluid transport by local osmosis does not change significantly (Fig. 8). In contrast, the electro-osmosis model predicts a decrease in fluid transport as a function of Na^+ channel inhibition, due to the decreasing paracellular cation flow. The experimental data for the effect of phenamil on transendothelial fluid transport again are in close agreement with the prediction of the electro-osmosis model, and not with that of local osmosis.

Cl^- Channel Inhibitors. Simulating the effects of Cl^- channel inhibitors by setting the relative permeability of this element to zero, results in the prediction of a slightly reduced fluid transport by the model, as shown in Fig. 9. The predictions based on the assumption of electro-osmosis are in excellent quantitative agreement with the experimental data presented by Diecke et al. 2004. On the other hand, assuming local osmosis leads to the prediction of a much larger decrease in fluid transport (Fig. 9).

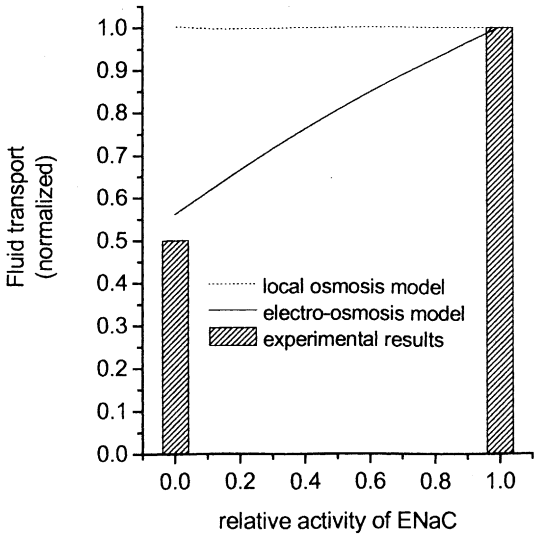

Fig. 8. Effect of inibition of apical Na^+ channels by phenamil on translayer fluid transport. Comparison of the prediction of the N2B model assuming fluid transport by local osmosis (*dotted line*) and by electro-osmosis, with fluid transport determined experimentally (Kuang, Cragoe & Fischbarg, 1993) as mentioned in the legend to Fig. 7.

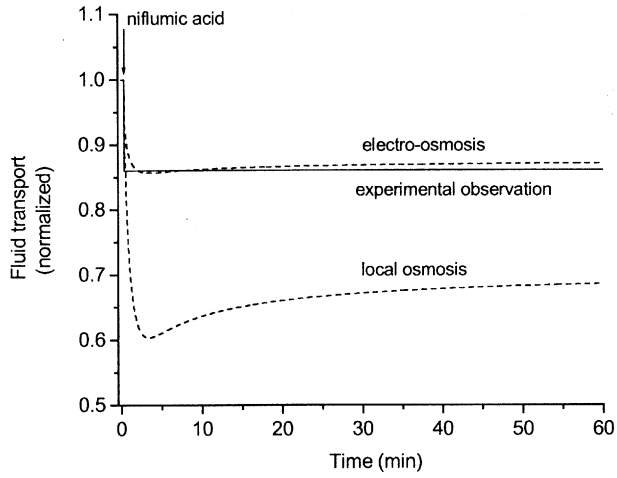

Fig. 9. Effect of inhibition of Cl^- channels on translayer fluid transport. Comparison of the model output with experimental data on fluid transport (Diecke et al., 2004) determined from changes in corneal thickness (Dikstein & Maurice, 1972).

Ionic Replacements

Bicarbonate. We have simulated the effects of replacement of HCO_3^- with Cl^- ions on the transendothelial potential difference and on fluid transport. As shown in Fig. 10 (upper panel), the potential difference decreases as a function of extracellular [HCO_3], in agreement with the experimental observations (Fischbarg & Lim, 1974). In the lower panel of Fig. 10, we have compared the model predictions for the complete replacement of extracellular HCO_3^- with Cl^- on fluid transport with experimental observations reported by Kuang (Kuang et al., 1990). Again, the predictions based on electro-osmotic fluid transport are in close agreement with the experimental data, while those based on local osmosis are significantly different.

Sodium Replacement. We simulated the effect of replacing extracellular Na^+ with a cell impermeant ion on the transendothelial potential difference. Figure 11 compares the results of this simulation with data reported by Fischbarg (Fischbarg & Lim, 1974). The agreement between model predictions and experimental observations is good.

Chloride Replacement. Figure 12 shows the results of a bilateral replacement of the ambient Cl^- with a cell impermeant anion (which may be thought of as methanesulfonate). We also assumed a correspondingly lesser Goldman permeability through the tight junction for the replacing anion, about 28% of that of Cl^-. Experimentally, it was observed (Fischbarg & Lim, 1974) that subsequent to that exchange the corneal thickness evidenced rapid decrease, presumably due to an osmotic shift, followed by a slower increase probably related to the effect of lack of Cl^- on the fluid pump. Figure 12 reproduces the experimental delayed rise in corneal thickness referred to, as well as the predictions for electro-osmotic and local osmotic fluid transport. As can be seen, both predictions fit the findings reasonably well.

Discussion

General Characteristics of the Model for the Steady State

Electrolyte Movements

We present here a mathematical model of electrolyte and fluid transport across the corneal endothelium. The model incorporates the ion channels and transporters so far described for the corneal endothelium (Fig. 1). To highlight some of the main elements, the cell would take up HCO_3^- via a basolateral NBC operating at 2:1 stoichiometry, and would extrude HCO_3^- across the apical membrane via a Na^+-HCO_3^- cotransporter operating at 3:1 stoichiometry, as recently proposed (Diecke et al., 2004). The model also incorporates an apical epithelial Na^+ channel (ENaC), which would provide a path for recirculation of a fraction of the paracellular Na^+ flow; the limb for Na^+ movement would be completed by the Na^+ pump extruding this cation through the basolateral membrane.

The model provides a detailed picture of the electrolyte movement during the steady state (Figs. 2,

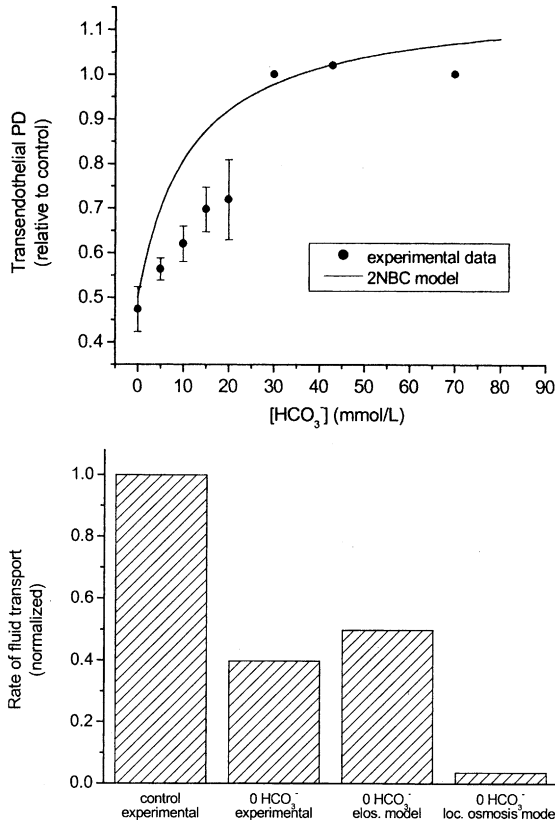

Fig. 10. *Top*: Transendothelial electrical potential difference as a function of the ambient HCO_3^- concentration. Experimental data and their error bars are from Fischbarg & Lim (1974). *Bottom*: Rate of fluid transport across corneal endothelium (Dikstein & Maurice, 1972). The effect of replacing all ambient HCO_3^- by Cl^-, as reported in Kuang et al. (1990), is compared to predictions from the two indicated versions of the model.

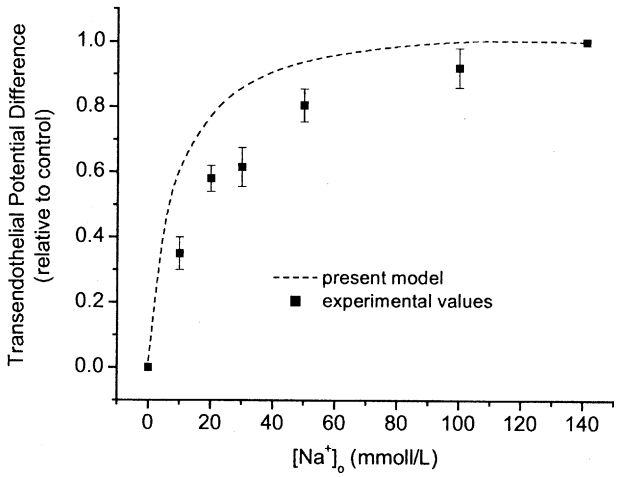

Fig. 11. Transendothelial electrical potential difference as a function of the ambient sodium concentration. The predictions of the model are compared to experimental data reproduced from Fischbarg & Lim (1974).

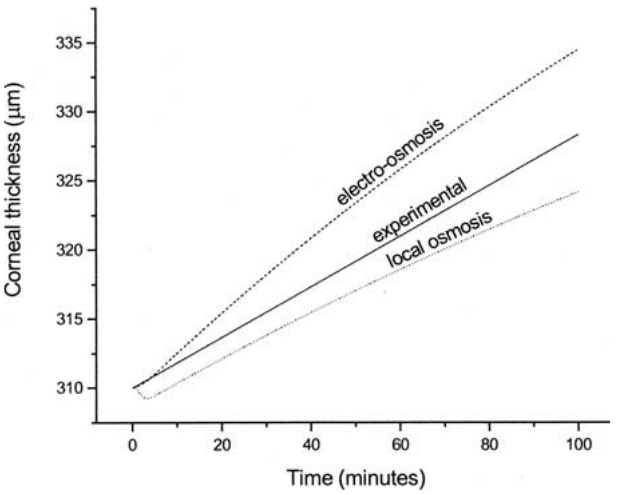

Fig. 12. In the experimental data shown, ambient Cl^- was replaced with sulfate^{2-} (Fischbarg & Lim, 1974). For the simulations, external Cl^- was replaced with an impermeant anion.

5). It predicts a transcellular flux of HCO_3^- of 0.88 μmol cm^{-2} h^{-1} from basolateral to apical side (Figs. 2, 5) and a comparatively small paracellular flux in the opposite direction of 0.08 μmol cm^{-2} h^{-1} for a net transendothelial HCO_3^- flux of 0.80 μmol cm^{-2} h^{-1} (Fig. 5). This value is in reasonable agreement with experimentally determined fluxes of 0.53 μmol cm^{-2} h^{-1} across cultured bovine corneal endothelial cell layers (Diecke et al., 2004) and 0.67 μmol cm^{-2} h^{-1} across rabbit corneal endothelium (Hodson & Miller, 1976).

There is also (Fig. 2) a transcellular Cl^- flux (from basolateral to apical) of 0.16 μmol cm^{-2} h^{-1}. However, due to a larger Cl^- flux through the paracellular pathway (0.22 μmol cm^{-2} h^{-1}) in the opposite direction (Fig. 5), there is only a small net translayer Cl^- flux of 0.06 μmol cm^{-2} h^{-1} from the apical to the basolateral side. The model predicts both transcellular and paracellular K^+ fluxes (Figs. 2, 5) from the basolateral to the apical side for a net flux of 0.35 μmol cm^{-2} h^{-1}. The transcellular Na^+ flux (0.24 μmol cm^{-2} h^{-1}), in contrast to all other ions, proceeds from the apical to the basolateral side (Fig. 2), while 0.63 μmol cm^{-2} h^{-1} of Na^+ flow from the basolateral to the apical side through the paracellular pathway (Fig. 5).

Strikingly, the net transcellular flux is almost entirely an anion flux, about 1.04 μmol cm^{-2} h^{-1} (Fig. 5). The movement of cations through the cell is just 0.093 μmol cm^{-2} h^{-1}, or only some 10% of the anion flux. Net transport of salt across the layer takes place only because of the paracellular movement of cation (Fig. 5), driven by the electrical field. This pattern of events coincides precisely with experimental evidence; in the Hodson laboratory results (Hodson & Miller, 1976), there was a net Na^+ flux across the endothelial layer only at open circuit; short-circuiting the layer eliminated that net movement.

Fluid Transport

The model also computes fluid transport based on two mechanisms of solute-solvent coupling: (a) near isotonic fluid movement due to local osmosis, and (b) electro-osmotic coupling of fluid to the current flow through electrically charged tight junctions. Evidence for the latter mechanism was provided recently by Sanchez et al. (2002). As mentioned in the Results section, for an undisturbed or reference endothelial layer, the present model correctly predicts the amounts transported experimentally by endothelial preparations (4 to 6 μL hr^{-1} cm^{-2}, (Maurice, 1984)).

Varying Degrees of Compliance for the Model

The model works satisfactorily over a range of intracellular concentrations. For instance, setting the intracellular concentrations to values approximating those postulated by Bonanno (Bonanno & Giasson, 1992b) ($[Na^+]_i$ = 30 mM, $[K^+]_i$ = 115 mM, $[Cl^-]_I$ = 55 mM, and $[HCO_3^-]_I$ = 22 mM) results in a somewhat reduced fluid transport of 4.1 and 4.3 μL hr^{-1} cm^{-2} for electro-osmotic and local osmotic coupling, respectively (*data not shown*). Both of these values are well within the range of experimentally obtained values. In contrast, there are some areas for which the model has little or no compliance. One interesting issue in this regard is that posed by the comparatively low activity for the Cl^- channel assumed in this context (Fig. 2). It may be argued there could be other epithelia in which most of the transcellular anion flux would be made up of Cl^- rather than $HCO3^-$, and that would be accompanied by high turnover or permeability for the Cl^- channels. However, at least for the present case, Cl^- channel turnover has to be defined only within narrow limits, as discussed in the Results section and exemplified in Fig. 3. To reiterate (Fig. 3), increase or decrease of the value chosen here for the Cl^- channel turnover leads to unphysiological reversals in the direction of Cl^- movement across the NKCC and the anion exchanger, respectively.

Perturbations of the Steady State

Effects of Inhibitors

Ouabain. We have simulated the effects of inhibitors by changing the relative permeability for relevant parameters. Figures 6 to 12 represent examples of such perturbations. Fig. 6 shows a selection of model output for several important cellular characteristics after ouabain inhibition is simulated. Aside from the expected changes in the electrolytes transported by the Na^+ pump, the volume increases as the concentrations shift towards the Donnan equilibrium resulting from the presence of fixed impermeant intracellular anions.

Other Inhibitors

DIDS. The results of this simulation are shown in Fig. 7, and constitute perhaps the most striking ones in this context. DIDS is assumed to inhibit (a) Cl^- channels, (b) NBCs, and (c) the anion exchanger. Here and elsewhere, to avoid divisions by zero, "total" inhibition was set to mean 99.9% inhibition for all of these. As mentioned in the Results section, the model predictions (Fig. 7) agree with the experimental results only if electro-osmosis (and not local osmosis) is assumed.

Phenamil. The conclusions here are the same as those above, namely, the experimental data (Fig. 8) agree with electro-osmosis, and not with local osmosis.

Cl^- Channel Inhibitors. Once more, the same conclusion is drawn (Fig. 9) in favor of electro-osmosis.

Effects of Ionic Replacements

Replacement of ambient $HCO3^-$ (by Cl^-) leads to the same conclusion (Fig. 10, bottom panel): the experimental data (Fischbarg & Lim, 1974) agree with electro-osmosis much better than with local osmosis. The upper panel shows that the model closely predicts the behavior of the transendothelial *PD*. As can be seen there, half-maximal effects for the experimental data appear to fall between 10 and 20 mM of the anion. That is also the range of the *K*m values for the HCO_3^- sites in the N2B and N3B cotransporters (Table 3).

The model simulations also generate a reasonable fit for the effect of ambient Na^+ on the transendothelial *PD* (Fig. 11) recorded experimentally (Fischbarg & Lim, 1974). The transendothelial *PD* is a hyperbolic function of the ambient $[Na^+]$, with an apparent *K*m of 20 mM (experimental) *vs.* 9 mM (simulation). An explanation for this effect would include saturable effects on the NBC cotransporters and the Na^+ pump.

Lastly, Fig. 12 shows that the model predicts the experimentally observed (Fischbarg & Lim, 1974) behavior of the transport system and the consequent increase in corneal hydration resulting from replacing ambient Cl^- by SO_4^{2-}. No distinction between the two competing models can be drawn from these data.

Conclusions and Predictions from the Mathematical Model

In conclusion, our mathematical model of the corneal endothelium, based largely on data obtained on

rabbit cornea and cultured layers of bovine corneal endothelial cells, simulates quite accurately many experimental findings for the steady and nonsteady states. However there is one specific variant of the model that fits the results best: electro-osmosis. For the overwhelming majority of the simulations, whether it is about DIDS, phenamil, or Cl^- channel inhibitors, only the electro-osmosis model predicts a close fit to the experimental data.

The model also predicts a number of parameters that can be tested experimentally. These include changes in intracellular electrolytes, cell volume, cell pH, membrane potential, transcellular potential difference and transendothelial fluid transport. Lastly, the model permits expansion to include the regulation of the function of individual elements by cell signaling compounds. The model, thus, can serve as the basis for a comprehensive description and explanation of the function of the corneal endothelial fluid pump in steady and nonsteady states.

Appendix

We reproduce below the kinetic principles on which we based the calculations of the respective driving forces for each of the model elements. All driving forces used in the program were normalized to be dimensionless. Symbols used in the Appendix are:

N, K, C, B, H	Sodium, Potassium, Chloride, Bicarbonate, Hydrogen identifiers
n, k, c, b, h	Identifying ions in line above, but used as subindices
o, i	subindices identifying: *o*, outside the cell; *i*, intracellular
No, Ni	Sodium concentration
Ko, Ki	Potassium concentration
Co, Ci	Chloride concentration
Bo, Bi	Bicarbonate concentration
Ho, Hi	Hydrogen ion concentration
kn, kk, kc, kb, kh	Dissociation constants for given ions and different carriers
Eo	Free carrier concentration on the outside of the cell membrane
Ei	Free carrier concentration on the inside of the cell membrane
Et	Total carrier concentration
J	chemical flux
U1	Absolute apical intracellular potential
u1	normalized ('reduced') apical intracellular potential, u1 = U1 F/(RT)
U2	Absolute basolateral intracellular potential
u2	Normalized ('reduced') basolateral intracellular potential, u2 = U2 F/(RT)
n, m	Number of charges for cations and anions, respectively
z, w	Signed charges for cations and anions, respectively
P	Permeability
f	Several intermediate expressions
Num	Numerator
Den	Denominator
Q	Intermediate expression

Cl^-/HCO_3^- Exchanger

$Eo + Co = EoC$ $\quad EoC = Eo \cdot Co/kc$

$Eo + Bo = EoB$ $\quad EoB = Eo \cdot Bo/kb$

$Ei + Ci = EiC$ $\quad EiC = Ei \cdot Ci/kc$

$Ei + Bi = EiB$ $\quad EiB = Ei \cdot Bi/km$

$Et = Eo + EoC + EoB + Ei + EiB + EiC$

$Et = Eo \cdot (1 + Co/kc + Bo/kb) + Ei \cdot (1 + Ci/kc + Bi/kb)$

$P \cdot Eo \cdot (Co/kc + Bo/kb) = P \cdot Ei \cdot (Ci/kc + Bi/kb)$

$Eo/Ei = (Co/kc + Bo/kb)/(Ci/kc + Bi/kb) = Q$

$Eo = Et/((1 + Co/kc + Bo/kb) + ((Co/kc + Bo/kb)/(Ci/kc + Bi/kb)) \cdot (1 + Ci/kc + Bi/kb))$

$Ei = Et/(((Ci/kc + Bi/kb)/(Co/kc + Bo/kb)) \cdot (1 + Co/kc + Bo/kb + 1 + Ci/kc + Bi/kb)$

Fluxes can be calculated using permeabilities.

$Jb\ (out) = P \cdot Ei \cdot Bi/kb;$ $\quad Jb(in) = P \cdot Eo \cdot Bo/kb;$

$Jb\ (net) = P \cdot (Ei \cdot Bi - Eo \cdot Bo)/kb$

$Jc(net) = -Jb(net)$

Na^+/H^+ Exchanger

$Eo + No = EoN$ $\quad EoN = Eo \cdot No\ /\ kn$

$Eo + Ho = EoH$ $\quad EoH = Eo \cdot Ho\ /\ kh$

$Ei + Ni = EiN$ $\quad EiN = Ei \cdot Ni\ /\ kn$

$Ei + Hi = EiH$ $\quad EiH = Ei \cdot Hi\ /\ kh$

$Et = Eo + EoN + EoH + Ei + EiN + EiH$

$Et = Eo \cdot (1 + No\ /\ kn + Ho\ /\ kh) + Ei \cdot (1 + Ni\ /\ kc + Hi\ /\ khb)$

$P \cdot Eo \cdot (No\ /\ kn + Ho\ /\ kh) = P \cdot Ei \cdot (Ni\ /\ kn + Hi\ /\ kh)$

$Eo\ /\ Ei = (No\ /\ kn + Ho\ /\ kh)\ /\ (Ni\ /\ kn + Hi\ /\ kh) = Q$

$Eo = Et\ /\ ((1 + No\ /\ kn + Ho\ /\ kh) + ((No\ /\ kn + Ho\ /\ kh)\ /\ (Ni\ /\ kn + Hi\ /\ kh)) \cdot (1 + Ni\ /\ kn + Hi\ /\ kn))$

$Ei = Et\ /\ (((Ni\ /\ kn + Hi\ /\ kh)\ /\ (Ko\ /\ kn + Ho\ /\ kh)) \cdot (1 + No\ /\ kn + Ho\ /\ kh) + (1 + Ni\ /\ kn + Hi\ /\ kh))$

$Jn(in) = P \cdot Eo \cdot No\ /\ kn;$ $\quad Jn(out) = P \cdot Ei \cdot Ni\ /\ kn$

$Jn(net) = Jn(in) - Jn(out) = P \cdot (Eo \cdot No - Ei \cdot Ni)\ /\ kn$

$Jh(net) = -Jn(net)$

NKCC Cotransporter

$EoN = Eo \cdot No / kn$
$EoNC = Eo \cdot No \cdot Co / (kn \cdot kc)$
$EoNCK = Eo \cdot No \cdot CoKo / (kn \cdot kc \cdot kc)$
$EoNKC2 = Eo \cdot No \cdot Ko \cdot Co^2 / (kn \cdot kk \cdot kc^2)$

$EiN = Ei \cdot Ni / kn$
$EiNC = Ei \cdot Ni \cdot Ci / (kn \cdot kc)$
$EiNCK = Ei \cdot Ni \cdot Ci \cdot Ki / (kn \cdot kc \cdot kk)$
$EiNKC2 = Ei \cdot Ni \cdot Ki \cdot Ci^2 / (kn \cdot kk \cdot kc^2)$

Conservation equation:
$Et = Eo + EoN + EoNK + EoNKC2 + Ei + EiN + EiNK + EiNKC2$
Total amount of carrier (bound plus free) entering the cell must equal that leaving the cell.
$P_1 \cdot EoNKC2 + P_2 Eo = P_1 EiNKC2 + P_2 Ei$
$P_2 = r \cdot P_1$
$Eo \cdot (P_1 \cdot No \cdot Ko \cdot Co^2 / (kn \cdot kk \cdot kc^2) + r \cdot P_1) = Ei \cdot (P_1 Ni \cdot Ki \cdot Ci^2 / (kn \cdot kk \cdot kc^2) + r \cdot P_1)$
$Ei = Eo \cdot (No \cdot Ko \cdot Co^2 / (kn \cdot kk \cdot kc^2) + r) / (Ni \cdot Ki \cdot Ci^2 / (kn \cdot kk \cdot kc^2) + r)$
$Eo = Ei \cdot (Ni \cdot Ki \cdot Ci^2 / (kn \cdot kk \cdot kc^2) + r) / (No \cdot Ko \cdot Co^2 / (kn \cdot kk \cdot kc^2) + r)$
$Ei / Eo = Q = (No \cdot Ko \cdot Co^2 / (kn \cdot kk \cdot kc^2) + r) / (Ni \cdot Ki \cdot Ci^2 / (kn \cdot kk \cdot kc^2) + r)$
$Num1 = P_1 \cdot Et \cdot No \cdot Ko \cdot Co^2 / (kn \cdot kkk \cdot kc^2)$
$Den1 = (1 + No / kn + No \cdot Ko / kn \cdot kk) + No \cdot Ko \cdot Co^2 / (knkkkc^2) + (No \cdot Ko \cdot Co^2 / (kn \cdot kk \cdot kc^2) + r) / (Ni \cdot Ki \cdot Ci^2 / (kn \cdot kk \cdot kc^2) + r) \cdot (1 + Ni / kn + Ni \cdot Ki / (kn \cdot kk) + Ni \cdot Ki \cdot Ci^2 / (kn \cdot kk \cdot kc^2)$
$Num2 = P_1 \cdot Et \cdot Ni \cdot Ki \cdot Ci^2 / (kn \cdot kk \cdot kc^2)$
$Den2 = (1 + Ni / kn + Ni \cdot Ki / (kn \cdot kk) + Ni \cdot Ki \cdot Ci^2 / (kn \cdot kk \cdot kc^2) + (Ni \cdot Ki \cdot Ci^2 / (kn \cdot kk \cdot kc^2) + kr) / (No \cdot Ko \cdot Co^2 / (kn \cdot kk \cdot kc^2) + kr) \cdot (1 + No / kn + No \cdot Ko / (kn \cdot kk) + No \cdot Ko \cdot Co^2 / (knkkkc^2)$
$Jnet = P \cdot (Num1 / Den1 - Num2 / Den2)$

Na-2HCO_3 Cotransporter

$n = 1 : z = 1 : m = 2 : w = -1$
$f3 = exp((n \cdot z + m \cdot w) \cdot u^2)$
$f4 = u2 / (1 - f3)$
$EoN = E \cdot No / kn$
$EoNB2 = Eo \cdot Bo^2 / (kn \cdot kb^2)$

$EiN = Ei \cdot Ni \cdot / kn$
$EiNB2 = Ei \cdot Ni \cdot Bi^2 / (kn \cdot kb^2)$

Conservation equation:
$Et = Eo + EoN + EoNB2 + Ei + EiN + EiNB2$
$Pi \cdot Eo \cdot No \cdot Bo^2 / (kn \cdot kb^2) + P_2 \cdot Eo = P_1 \cdot (Ei \cdot Ni \cdot Bi^2 / (kn \cdot kb^2)) \cdot f3 + P_2 \cdot Ei$
$P_2 = r \cdot Pi$
$f2 \cdot Eo \cdot No \cdot Bo^2 / (kn \cdot kb^2) + r \cdot Eo = f2 \cdot (Ei \cdot Ni \cdot Bi^2 / (kn \cdot kb^2)) \cdot f3 + r \cdot Ei$
$Eo \cdot (f4 \cdot No \cdot Bo^2 / (kn \cdot kb^2) + r) = Ei \cdot (f4 \cdot Ni \cdot Bi^2 / (kn \cdot kb^2) \cdot f3 + r)$
$Eo / Ei = (f4 \cdot Ni \cdot Bi^2 \cdot f3 / (kn \cdot kb^2) + r) / (f4 \cdot No \cdot Bo^2 / (kn \cdot kb^2 + r) = Q$
$Ei / Eo = (f4 \cdot No \cdot Bo^2 / (kn \cdot kb^2) + r) / (f4 \cdot Ni \cdot Bi^2 \cdot f3 / (kn \cdot kb^2) + r) = 1 / Q$
$Jin = P_1 \cdot f4 \cdot (No \cdot Bo^2 / (1 \cdot kb^2)) / (1 + No / kn + NoBo^2 / (kn \cdot kb^2) + (1 + Ni / kn + Ni \cdot Bi^2 / (kn \cdot kb^2) \cdot Q$
$Jout = P_1 \cdot f4 \cdot Ei \cdot Ni \cdot Bi^2 / (kn \cdot kb^2) \cdot f3 / (1 + Ni / kn + Ni \cdot Bi^2 / (kn \cdot kb^2) + (1 + No / kn + NoBo^2 / (kn \cdot kb^{\wedge}2) \cdot 1 / Q$
$Jnet = Jin - Jout$

Na-3HCO_3 Cotransporter

$n = 1 : z = 1 : m = 3 : w = -1$
$f1 = exp((n \cdot z + m \cdot w) \cdot u1)$
$f2 = u1 / (1 - f1)$
$EoN = E \cdot No / kn$
$EoNB2 = Eo \cdot Bo^3 / (kn \cdot kb^3)$

$EiN = Ei \cdot Ni \cdot / kn$
$EiNB2 = Ei \cdot Ni \cdot Bi^3 / (kn \cdot kb^3)$

Conservation equation:
$Et = Eo + EoN + EoNB3 + Ei + EiN + EiNB3$
$P_1 \cdot Eo \cdot No \cdot Bo^3 / (kn \cdot kb^3) + P_2 \cdot Eo = P_1 \cdot (Ei \cdot Ni \cdot Bi^3 / (kn \cdot kb^3)) \cdot f1 + P_2 \cdot Ei$
$P_2 = r \cdot Pi$
$f2 \cdot Eo \cdot No \cdot Bo^2 / (kn \cdot kb^2) + r \cdot Eo = f2 \cdot (Ei \cdot Ni \cdot Bi^2 / (kn \cdot kb^2)) \cdot f3 + r \cdot Ei$
$Eo \cdot (f4 \cdot No \cdot Bo^2 / (kn \cdot kb^2) + r) = Ei \cdot (f4 \cdot Ni \cdot Bi^2 / (kn \cdot kb^2) \cdot f3 + r) \cdot Ei$
$Eo / Ei = (f4 \cdot Ni \cdot Bi^2 \cdot f3 / (kn \cdot kb^2) + r) / (f4 \cdot No \cdot Bo^2 / (kn \cdot kb^2 + r) = Q$
$Ei / Eo = (f4 \cdot No \cdot Bo^2 / (kn \cdot kb^2) + r) / (f4 \cdot Ni \cdot Bi^2 \cdot f3 / (kn \cdot kb^2) + r) = 1 / Q$
$Jin = P_1 \cdot f4 \cdot (No \cdot Bo^2 / (kn \cdot kb^2)) / (1 + No / kn + NoBo^2 / (kn \cdot kb^2) + (1 + Ni / kn + Ni \cdot Bi^2 / (kn \cdot kb^2) \cdot Q$
$Jout = P_1 \cdot f4 \cdot Ei \cdot Ni \cdot Bi^2 / (kn \cdot kb^2) \cdot f3 / (1 + Ni / kn + Ni \cdot Bi^2 / (kn \cdot kb^2) + (1 + No / kn + NoBo^2 / (kn \cdot kb^2) \cdot 1 / Q$
$Jnet = Jin - Jout$

K^+ Channel

Basolateral

$n = 1 : z = 1 : m = 0 : w = 0$

$f3 = exp\,((n \cdot z + m \cdot w) \cdot u2)$

$f4 = -(n \cdot z + m \cdot w) \cdot u2 / (1 - f3)$

$J(net) = Pk \cdot f4 \cdot (Ko - Ki \cdot f3)$

Apical

$n = 1 : z = 1 : ni = 0 : w = 0$

$f1 = exp\,((n \cdot z + m \cdot w) \cdot u1)$

$f2 = -n \cdot z \cdot u1 / (1 - f1)$

$J(net) = Pk \cdot f2 \cdot (Ko - Ki \cdot f1)$

Cl^- Channel

$n = 0 : z = 0 : m = 1 : w = -1$

$f1 = exp\,((n \cdot z + m \cdot w) \cdot u1)$

$f2 = -m \cdot w \cdot u1 / (1 - f1)$

$J(net) = Pc1 \cdot f2 \cdot (Co - Ci \cdot f1)$

Na^+ Channel

$n = 1 : z = 1 : m = 0 : w = 0$

$f1 = exp\,((n \cdot z + m \cdot w) \cdot u1)$

$f2 = -n \cdot z \cdot u1 / (1 - f1)$

$J(net) = Pna \cdot f2 \cdot (No - Ni \cdot f1))$

H^+–ATPase

$J_H = P_H \cdot (u1 + DpH + U_{pump})$;

U_{pump} = electrochemical energy of the pump, assumed to be 120 mV (Verkman & Alpern, 1987).

Na^+-K^+-ATPase

$fp = u2 \cdot 26.8 - 200$

$Jn \cdot = Pn \cdot fp \cdot (Ni / (Ni + kn))^3 \cdot (Ko / (Ko + kk))^2$

(Verkman & Alpern, 1987).

We thank Drs. A.S. Verkman and N. Illsley for generously providing the code of the Verkman laboratory epithelial model program (Hartmann & Verkman, 1990; Verkman & Alpern, 1987). Our work was supported by NIH Grant EY06178 (JF), and in part by Research to Prevent Blindness, Inc.

References

Aronson, P.S., Suhm, M.A., Nee, J. 1983. Interaction of external H^+ with the Na^+-H^+ exchanger in renal microvillus membrane vesicles. *J. Biol. Chem.* **258:**6767–6771

Bonanno, J.A. 2003. Identity and regulation of ion transport mechanisms in the corneal endothelium. *Prog. Retin. Eye Res.* **22:**69–94

Bonanno, J., Giasson, C. 1992a. Intracellular pH regulation in fresh and cultured bovine corneal endothelium.I. Na^+ H^+ Exchange in the absence and prescence of $HCO3^-$ Invest Ophthalmol. *Vis. Sci.* **33:**3058–3067

Bonanno, J.A., Giasson, C. 1992b. Intracellular pH regulation in fresh and cultured bovine corneal endothelium. II. Na^+:H-$CO3^-$ cotransport and Cl-$HCO3^-$ exchange. *Invest. Ophthalmol. Vis. Sci.* **33:**3068–3079

Diecke, F.P., Wen, Q., Iserovich, P., Li, J., Kuang, K., Fischbarg, J. 2005. Regulation of Na-K-2Cl cotransport in cultured bovine corneal endothelial cells. *Exp. Eye Res.* (in press)

Dikstein, S., Maurice, D.M. 1972. The metabolic basis of the fluid pump in the cornea. *J. Physiol.* **221:**29–41

Fischbarg, J. 1979. Pathways for water permeation across epithelia. *In:* Bourguet, J, Chevalier, V, Parisi, M, Ripoche, P., (eds.) Hormonal Control of Epithelial Transport. pp 323–334, INSERM, Paris

Fischbarg, J., Hernandez, J.A., Liebovitch, L.S., Koniarek, J.P. 1985. The mechanism of fluid and electrolyte transport across corneal endothelium: critical revision and update of a model. *Curr. Eye Res.* **4:**351–360

Fischbarg, J., Lim, J.J. 1974. Role of cations, anions and carbonic anhydrase in fluid transport across rabbit corneal endothelium. *J. Physiol.* **241:**647–675

Grichtchenko, II., Romero, M.F., Boron, W.F. 2000. Extracellular HCO_3^- dependence of electrogenic Na/HCO_3 cotransporters cloned from salamander and rat kidney. *J. Gen. Physiol.* **115:**533–546

Gross, E., Hopfer, U. 1998. Voltage and cosubstrate dependence of the Na-HCO_3 cotransporter kinetics in renal proximal tubule cells. *Biophys. J.* **75:**810–824

Hartmann, T., Verkman, A.S. 1990. Model of ion transport regulation in chloride-secreting airway epithelial cells. Integrated description of electrical, chemical, and fluorescence measurements. *Biophys. J.* **58:**391–401

Hodson, S., Miller, F. 1976. The bicarbonate ion pump in the endothelium which regulates the hydration of the rabbit cornea. *J. Physiol.* **263:**563–577

Jelamskii, S., Sun, X.C., Herse, P., Bonanno, J.A. 2000. Basolateral Na^+-K^+–$2Cl^-$ cotransport in cultured and fresh bovine corneal endothelium. *Invest. Ophthalmol. Vis. Sci.* **41:**488–495

Jentsch, T.J., Korbmacher, C., Janicke, I., Fischer, D.G., Stahl, F., Helbig, H., Hollwede, H., Cragoe, E.J. Jr., Keller, S.K., Wiederholt, M. 1988. Regulation of cytoplasmic pH of cultured bovine corneal endothelial cells in the absence and presence of bicarbonate. *J. Membrance Biol.* **103:**29–40

Kaye, G.I., Cole, J.D., Donn, A. 1965. Electron microscopy: sodium localization in normal and ouabain-treated transporting cells. *Science* **150:**1167–1168

Kedem, O., Katchalsky, A. 1958. Thermodynamic analysis of the permeability of biological membranes to non-electrolytes. *Biochim. Biophys. Acta* **27:**229–236

Kohn, O.F., Mitchell, P.P., Steinmetz, P.R. 1990. Characteristics of apical Cl-HCO_3 exchanger of bicarbonate-secreting cells in turtle bladder. *Am. J. Physiol.* **258:**F9–F14

Kuang, K., Cragoe, E.J., Fischbarg, J. 1993. Fluid transport and electroosmosis across corneal endothelium. *In:* Ussing, H.H, Fischbarg, J, Sten Knudsen, E, Hviid Larsen, E, Willumsen, N.J., (eds.) Proc. Alfred Benzon Symposium 34: Water Transport in Leaky Epithelia. pp 69–79, Copenhagen, Munksgaard

Kuang, K., Li, Y., Wen, Q., Wang, Z., Li, J., Yang, Y., Iserovich, P., Reinach, P.S., Sparrow, J., Diecke, F.P.J., Fischbarg, J. 2001. Corneal endothelial Na^+-K^+2Cl^- cotransporter: molecular identification, location, and contribution to fluid transport. *Am. J. Physiol.* **280:**C491–C499

Kuang, K., Li, Y., Yiming, M., Sanchez, J.M., Iserovich, P., Cragoe, E.J., Diecke, F.P., Fischbarg, J. 2004. Intracellular [Na^+], Na^+ pathways, and fluid transport in cultured bovine corneal endothelial cells. *Exp. Eye Res.* **79:**93–103

Kuang, K., Xu, M., Koniarek, J.P., Fischbarg, J. 1990. Effects of ambient bicarbonate, phosphate and carbonic anhydrase inhibitors on fluid transport across rabbit corneal endothelium. *Exp. Eye Res.* **50:**487–493

Lakshminarayanaiah, N. 1984. Equations of Membrane Biophysics. Academic Press, Orlando,

Latta, R., Clausen, C., Moore, L.C. 1984. General method for the derivation and numerical solution of epithelial transport models. *J. Membrance Biol.* **82:**67–82

Lew, V.L., Ferreira, H.G., Moura, T. 1979. The behaviour of transporting epithelial cells. I. Computer analysis of a basic model. Proc. R. Soc. Lond. *B. Biol Sci.* **206:**53–83

Lim, J.J., Fischbarg, J. 1981. Electrical properties of rabbit corneal endothelium as determined from impedance measurements. *Biophys. J.* **36:**677–695

Lim, J.J., Liebovitch, L.S., Fischbarg, J. 1983. Ionic selectivity of the paracellular shunt path across rabbit corneal endothelium. *J. Membrance Biol.* **73:**95–102

Maurice, D.M. 1984. The cornea and sclera. *In:* Davson, H., (eds.) The Eye. pp 1–158, Academic Press, Orlando, FL

Mullins, L.J., Noda, K. 1963. The influence of sodium-free solutions on the membrane potential of frog muscle fibers. *J. Gen. Physiol.* **47:**117–132

Novotny, J.A., Jakobsson, E. 1996. Computational studies of ion-water flux coupling in the airway epithelium. Construction of model. *Am. J. Physiol* **270 :**C 1751–1763

Peral, M.J., Calonge, M.L., Ilundain, A.A. 1995. Na^+-HCO_3^- transporter and intracellular pH regulation in chicken enterocytes. *Pfluegers Arch.* **430:**612–616

Rae, J.L., Dewey, J., Cooper, K., Gates, P. 1990. Potassium channel in rabbit corneal endothelium activated by external anions. *J. Membrane Biol.* **114:**29–36

Rae, J.L., Watsky, M.A. 1996. Ionic channels in corneal endothelium. *Am. J. Physiol.* **270:**C975–C989

Rimmer, S.J., Lane, J.R., Wigham, C.G., Hodson, S.A. 1999. Demonstration of a Na^+H^+ exchanger NHE1 in fresh bovine corneal endothelial cell basolateral plasma membrane. *Biochim. Biophys. Acta* **1419:**283–288

Sanchez, J.M., Li, Y., Rubashkin, A., Iserovich, P., Wen, Q., Ruberti, J.W., Smith, R.W., Rittenband, D., Kuang, K., Diecke, F.P.J., Fischbarg, J. 2002. Evidence for a central role for electro-osmosis in fluid transport by corneal endothelium. *J. Membrane Biol.* **187:**37–50

Sohma, Y., Gray, M.A., Imai, Y., Argent, B.E. 2000. HCO_3^- transport in a mathematical model of the pancreatic ductal epithelium. *J. Membrane Biol.* **176:**77–100

Sun, X.C., Bonanno, J.A., Jelamskii, S., Xie, Q. 2000. Expression and localization of Na^+-HCO_3 cotransporter in bovine corneal endothelium. *Am. J. Physiol.* **279:**C1648–C1655

Verkman, A.S., Alpern, R.J. 1987. Kinetic transport model for cellular regulation of pH and solute concentration in the renal proximal tubule. *Biophys. J.* **51:**533–546

Westenfelder, C., Earnest, W.R., Al-Bazzaz, F. 1980. Characterization of Na-K-ATPase in dog tracheal epithelium: enzymatic and ion transport measurements. *J. Appl. Physiol.* **48:**1008–1019

Wieth, J.O. 1979. Bicarbonate exchange through the human red cell membrane determined with [^{14}C] bicarbonate. *J. Physiol.* **294:**521–539

Wigham, C.G., Turner, H.C., Ogbuehi, K.C., Hodson, S.A. 1996. Two pathways for electrogenic bicarbonate ion movement across the rabbit corneal endothelium. *Biochim. Biophys. Acta* **1279:**104–110

Yang, D., Sun, F., Thomas, L.L., Offord, J., McCallum, D.K., Dawson, D.C., Hughes, B.A., Ernst, S.A. 2000. Molecular cloning and expression of an inwardly rectifying K^+ channel from bovine corneal endothelial cells. *Invest. Ophthalmol. Vis. Sci.* **41:**2936–2944